Progress In Electromagnetics Research, Vol. 116, 185–202, 2011

CHARACTERIZATION OF ANTENNA INTERACTION WITH SCATTERERS BY MEANS OF EQUIVALENT CURRENTS

C. G. González and Y. Álvarez López

Area of Signal Theory and Communications
University of Oviedo
Edif. Polivalente, Mod. 8, Campus Universitario de Viesques
E-33203, Gijón (Asturias), Spain

A. D. Casas

European Space Agency (ESA)
European Space Research and Technology Centre (ESTEC)
Noordwijk, The Netherlands

F. Las-Heras Andrés

Area of Signal Theory and Communications
University of Oviedo
Edif. Polivalente, Mod. 8, Campus Universitario de Viesques
E-33203, Gijón (Asturias), Spain

Abstract—Antenna characterization in presence of obstacles requires removing multipath effects in order to retrieve the non-distorted antenna radiation pattern. In this contribution a new approach based on the Sources Reconstruction Method is proposed. The idea is to characterize the Antenna-Under-Test (AUT) and the region where the scatterers are located through a set of equivalent currents. Finally, the reconstructed equivalent currents on the contour enclosing the AUT can be used to recover the AUT radiation pattern, removing most of the distortion effect due to the presence of the scatterers.

Received 8 February 2011, Accepted 20 April 2011, Scheduled 4 May 2011
Corresponding author: Yuri Álvarez López (yalopez@tsc.uniovi.es).

1. INTRODUCTION

Antenna measurement and characterization are affected by multiple sources of distortion, as for example, multipath effects due to signal reflection in the floor or walls of the measurement facility [1]. The effects of distortion in the measured radiation pattern are more significant in semi-anechoic chambers, and outdoor measurement facilities, where absorbers are not placed in all the surfaces.

Different methods have been proposed for multipath effect correction, being most of them based on Ultra-Wide-Band (UWB) channel characterization: the idea is to identify the reflected components in the time domain, then applying time domain gating to remove the non-desired contributions. Different procedures have been developed: [2] makes use of FFT and matrix-pencil methods, a correlation-based technique is described in [3], and [4] presents a narrowband technique based on recursive data.

Regarding this topic, the next improvement would be echo cancellation achievement when working at one single frequency. A well-known method is the so-called IsoFilter^{TM} technique [1, 5], based on spherical wave expansions, which allows the isolation of an individual radiation from multiple contributions that distort the measured radiation pattern. Another technique related to RCS measurements, based on the characterization of the contribution of two scatterers, is presented in [6].

Following the idea presented in [5] regarding the isolation of different radiators, this contribution proposes the introduction of an equivalent currents distribution to characterize the Antenna-Under-Test (AUT) and the surface/object where the signal is reflected. Assuming that the coupling effects between the object and the AUT are not significant, the non-distorted AUT pattern can be calculated by using the reconstructed equivalent currents on the AUT, i.e., taking out the equivalent currents that characterize the object.

The AUT and the object characterization by means of equivalent currents is achieved by using the Sources Reconstruction Method, an integral equation-based technique, which has been used for near-field to far-field transformation as well as for antenna diagnostics and characterization [7–12]. The equivalent currents-based AUT model can be applied for an accurate prediction of the radiated field in the AUT vicinity [13] as well as for the study of the antenna interaction with other structures, as explained in [14].

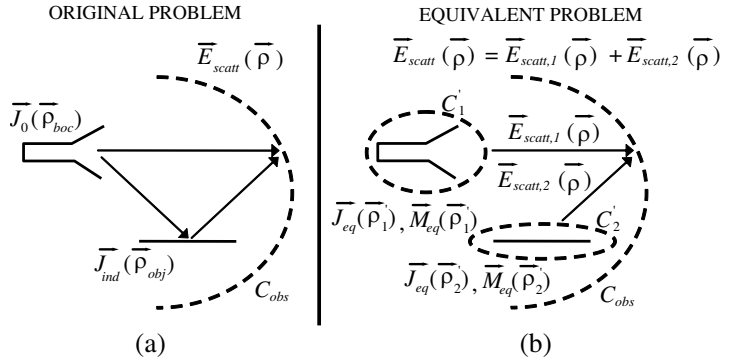

Figure 1. Antenna characterization in the presence of a scatterer. (a) Original problem. (b) Equivalent problem.

2. THE SOURCES RECONSTRUCTION METHOD

The Sources Reconstruction Method is based on the electromagnetic Equivalent Principle, allowing the replacement of the AUT by an equivalent currents distribution retrieved on a surface enclosing the AUT (see Fig. 1). The field in the outer region ($\vec{E}_{scatt}$) can be represented by the field generated by these equivalent currents distribution Eq. (1). For a two-dimensional problem and TM-polarization [15]:

$$E_{scatt}(\vec{\rho})\hat{z} = -\frac{k_0^{\eta}}{4}\hat{z}\int_{C_1'}\left\{H_0^{(2)}\left(k_0\left|\vec{\rho}-\vec{\rho}_1'\right|\right)\cdot\vec{J}_{eq}(\vec{\rho}_1')\cdot\hat{z}\right\}dC_1' - \frac{k_0}{4j}\int_{C_1'}\left\{H_1^{(2)}\left(k_0\left|\vec{\rho}-\vec{\rho}_1'\right|\right)\cdot\vec{M}_{eq}(\vec{\rho}_1')\times\frac{(\vec{\rho}-\vec{\rho}_1')}{|\vec{\rho}-\vec{\rho}_1'|}\right\}dC_1' \quad (1)$$

where $H_0^{(2)}$ is the Hankel function of 0-th order and second kind, η is the intrinsic impedance of the medium, k_0 is the wavenumber. C_1' is the contour enclosing the AUT. $\vec{\rho} = \vec{\rho}(x, y)$ is the vector defining the points where the field is observed, and $\vec{\rho}_1' = \vec{\rho}_1'(x_1', y_1')$, the vector defining the points where the currents are placed. $|\vec{\rho} - \vec{\rho}'|$ is defined as Eq. (2):

$$\left|\vec{\rho} - \vec{\rho}_1'\right| = \left(\left(x - x_1'\right)^2 + \left(y - y_1'\right)^2\right)^{1/2} \quad (2)$$

From the $\vec{E}_{scatt}$ calculated (or measured) on an acquisition contour C_{obs}, the $\vec{J}_{eq}(\vec{\rho}_1')$ and $\vec{M}_{eq}(\vec{\rho}_1')$ on C_1' are determined by solving the integral equations relating fields and sources Eq. (1).

Numerical solution of Eq. (1) is done by means of a 2D-Method-of-Moments (MoM), yielding a linear system of equations, $(E_{scatt}) = (Z) \cdot (J_{eq})$ (in matrix form). To solve it an iterative solver, the Conjugate Gradient method [16, 17], is proposed [8, 9]. The goal is to minimize a cost function relating the difference between the acquired scattered field and the field radiated by the equivalent currents Eq. (3).

$$\begin{pmatrix} \vec{E}_{scatt}(\vec{\rho}) \\ 0 \end{pmatrix} = \begin{pmatrix} Z_J(\vec{\rho};\vec{\rho}_1') & Z_M(\vec{\rho};\vec{\rho}_1') \\ Z_J(\vec{\rho}_1';\vec{\rho}_1') & Z_M(\vec{\rho}_1';\vec{\rho}_1') \end{pmatrix} \begin{pmatrix} \vec{J}_{eq}(\vec{\rho}_1') \\ \vec{M}_{eq}(\vec{\rho}_1') \end{pmatrix} \tag{3}$$

Note that the zero internal field condition is enforced to ensure that there is a correspondence between the reconstructed equivalent currents on C_1' and the tangential field components on that surface, as stated in [11, 12].

Once the AUT is characterized, next step is to consider the multipath contribution due to signal reflection on a scatterer. If an estimation of the placement and size of the scatterer is provided, an equivalent currents distribution $\vec{J}_{eq}(\vec{\rho}_2')$ and $\vec{M}_{eq}(\vec{\rho}_2')$ on C_2' are calculated by solving the following system of equations, Eq. (4):

$$\begin{pmatrix} \vec{E}_{scatt}(\vec{\rho}) \\ 0 \\ 0 \end{pmatrix} = \begin{pmatrix} Z_I(\vec{\rho};\vec{\rho}_1') & Z_I(\vec{\rho};\vec{\rho}_2') \\ Z_I(\vec{\rho}_1';\vec{\rho}_1') & Z_I(\vec{\rho}_1';\vec{\rho}_2') \\ Z_I(\vec{\rho}_2';\vec{\rho}_1') & Z_I(\vec{\rho}_2';\vec{\rho}_2') \end{pmatrix} \begin{pmatrix} \vec{I}_{eq}(\vec{\rho}_1') \\ \vec{I}_{eq}(\vec{\rho}_2') \end{pmatrix}$$

$$\vec{I}_{eq}(\vec{\rho}_1') = \begin{pmatrix} \vec{J}_{eq}(\vec{\rho}_1') \\ \vec{M}_{eq}(\vec{\rho}_1') \end{pmatrix}, \quad \vec{I}_{eq}(\vec{\rho}_2') = \begin{pmatrix} \vec{J}_{eq}(\vec{\rho}_2') \\ \vec{M}_{eq}(\vec{\rho}_2') \end{pmatrix} \tag{4}$$

$$Z_I(\vec{\rho};\vec{\rho}_m') = \begin{pmatrix} Z_J(\vec{\rho};\vec{\rho}_m') & Z_M(\vec{\rho};\vec{\rho}_m') \end{pmatrix}, \quad m = 1, 2$$

$$Z_I(\vec{\rho}_n';\vec{\rho}_m') = \begin{pmatrix} Z_J(\vec{\rho}_n';\vec{\rho}_m') & Z_M(\vec{\rho}_n';\vec{\rho}_m') \end{pmatrix}, \quad n, m = 1, 2$$

In Eq. (4), the zero internal field condition is enforced inside C_1' and C_2'. The reconstructed equivalent currents on C_2' radiate the same field as the induced currents on the scatterer surface (see Fig. 1).

Therefore, the acquired field $(\vec{E}_{scatt})$ is the sum of the field radiated by the AUT and the field reflected on the scatterer Eq. (5):

$$\vec{E}_{scatt}(\vec{\rho}) = \vec{E}_{scatt,1}(\vec{\rho}) + \vec{E}_{scatt,2}(\vec{\rho}) \tag{5}$$

Then, the reflection in the object can be characterized by $\vec{J}_{eq}(\vec{\rho}_2')$ and $\vec{M}_{eq}(\vec{\rho}_2')$ on C_2', while $\vec{J}_{eq}(\vec{\rho}_1')$ and $\vec{M}_{eq}(\vec{\rho}_1')$ on C_1' are used to characterize the AUT.

As mentioned before, if the coupling effects between the AUT and the scatterer were negligible, the AUT radiation pattern without the scatterer distortion will correspond to $\vec{E}_{scatt,1}(\vec{\rho})$, which is the field radiated by $\vec{J}_{eq}(\vec{\rho}_1')$ and $\vec{M}_{eq}(\vec{\rho}_1')$.

2.1. Method Refinement

Equivalent currents reconstruction from two independent domains supposes an increase on the degrees of freedom, so that the system of equations to be solved may be quite sensitive to noise. In order to overcome this problem, it is proposed the use of near-field data collected or calculated as close as the reconstruction domain. For this purpose, a near field-to-near field (NF-NF) transformation, also based on the Sources Reconstruction Method, is introduced as a previous step prior to the retrieval of the equivalent currents on both domains.

The resulting method consists on an two-step strategy, depicted in Fig. 2: first, the NF-NF transformation is done by means of an equivalent currents distribution retrieved on a domain (denoted as C_0') enclosing all the radiating elements. The reconstructed equivalent currents, $\vec{J}_{eq}(\vec{\rho}_0')$ and $\vec{M}_{eq}(\vec{\rho}_0')$, will radiate the same field as the original problem radiators outside C_0' domain, and so the near field in a region surrounding C_0' can be obtained.

In a second step, equivalent currents in domain C_1' and C_2'

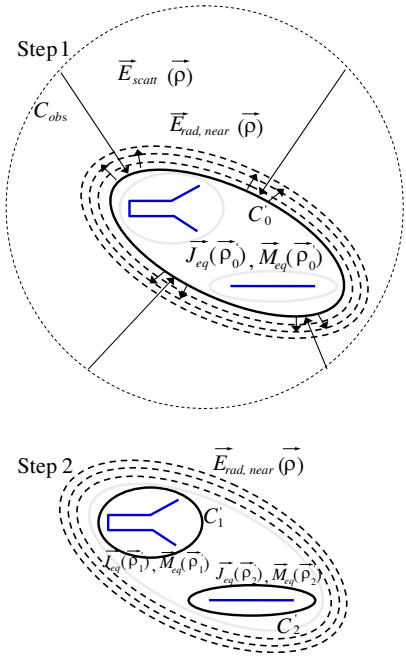

Figure 2. Method refinement using a two-step strategy. Black solid lines represent the reconstruction domain on each step.

are retrieved from the near field calculated around C_0', using the methodology described before (Eq. (4)).

3. APPLICATION EXAMPLES

Aiming to test the proposed method for multipath effects removal, three application examples are presented in this section. All cases are 2D, being the fields z-polarized (TM case) [14].

3.1. Horn Antenna Alone

The first example illustrates the SRM for antenna characterization. A horn antenna radiating in free space is selected as AUT, which is enclosed by an elliptical contour C_1'. The ellipse major axis is 8λ, the minor axis is 6λ, and it is centered at $x = 3\lambda$, $y = 0\lambda$ see Fig. 3).

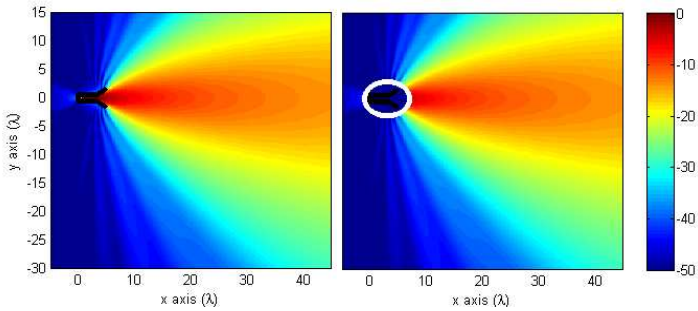

Figure 3. Electric field (normalized amplitude, in dB) (a) Original problem: horn antenna radiating in free space. (b) Equivalent problem: J_{eq} and M_{eq} on C_1' radiating in free space.

The field radiated by the AUT is acquired in a circumference of $R = 50\lambda(C_{obs})$. According to the field sampling criterion [18] the minimum number of field samples would be Eq. (6):

$$\begin{aligned} N &= \lceil k_0 R_0 + 10 \rceil = 42 \\ \Delta\varphi_{\min} &= 360^\circ/42 \approx 8^\circ \end{aligned} \tag{6}$$

where R_0 is the minimum radius of the circumference enclosing the AUT, that is $R_0 = 5\lambda$. Thus, the minimum sampling rate in the Observation Domain is 8°. It was decided to oversample, by taking a field sampling rate of $\Delta\varphi = 1^\circ$.

The equivalent currents are reconstructed on the elliptical contour (C_1') enclosing the horn antenna from the acquired field in the

observation domain (C_{obs}). The reconstruction domain (C_1') is discretized in 360 segments of variable length ($\Delta C_1'$) ensuring that $\Delta C_1' < 0.5\lambda$ ($\Delta C_1' = 0.24\lambda$ at most). Thus, the resulting matrix system has 1440 equations (360 field observation points +720 points inside C_1' where the zero internal field condition is enforced, as indicated in [11, 12]) and 720 unknowns (equivalent electric and magnetic currents).

The field radiated by the AUT and by the reconstructed $\vec{J}_{eq}(\vec{\rho}_1')$ and $\vec{M}_{eq}(\vec{\rho}_1')$ on C_1' is plotted in Fig. 2. No discrepancies between the radiated fields can be appreciated, which confirms the validity of the AUT model based on the equivalent currents.

3.2. Horn Antenna with Metallic Plate

In the second example, a metallic plate of 10λ (along x-direction) centered at $x = 30\lambda$ and $y = -20\lambda$ is placed in the measurement setup, trying to be realistic with a practical antenna measurement setup, as the one described in [19–21]. The field observation domain (C_{obs}) is the same as in the previous example.

Three reconstruction domains are considered in this example:

1) C_0', an ellipse containing both C_1' and C_2', as depicted in Fig. 4. The ellipse is centered at $x = 17\lambda$, $y = -10\lambda$, having a major

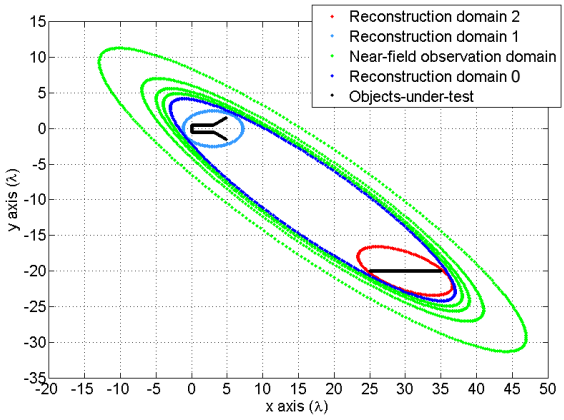

Figure 4. Domains on Example 2. Dark blue: C_0' reconstruction domain. Green: near-field observation domain. Dark blue: C_1' reconstruction domain. Red: C_2' reconstruction domain. Black: horn and metallic plate.

axis of 48λ, a minor axis of 10λ, and rotated 34.5°. The contour is discretized in 360 points, ensuring that $\Delta C_0' < 0.5\lambda$ (0.4λ at most).

2) C_1', the same as in the first example, enclosing the AUT.
3) C_2', another ellipse which encloses the metallic plate. The ellipse has a major axis of 14λ, a minor axis of 5λ, being centered at $x = 30\lambda$, $y = -20\lambda$. This elliptical contour is also discretized in 360 points, so that $\Delta C_2' < 0.15\lambda$.

The first step implies the solution of a system of equations having 1080 equations (360 field observation points +720 internal points where the zero internal field condition is enforced) and 720 unknowns (equivalent electric and magnetic currents). The near field is calculated in 4 ellipses concentric to C_0', and scaled by 1.05, 1.1, 1.2 and 1.5 factor (see Fig. 4).

Regarding the second step, a system of equations having 2880 equations (1440 near-field observation points +1440 internal points where the zero internal field condition is enforced) and 1440 unknowns (equivalent electric and magnetic currents in C_1' and C_2') has to be solved.

Results are plotted in Fig. 5. Fig. 5(a) corresponds to radiated fields of the original problem (horn antenna radiating in the presence of the metallic plate — the black line —), which is analyzed by means of a 2D-MoM.

Fields radiated by the equivalent currents reconstructed on C_0' are plotted in Fig. 5(b). It can be seen that, due to the enforcement of the zero internal field condition (Eq. (4)), the fields inside C_0' are zero, being the fields outside the reconstruction domain almost the same as in the original problem (Fig. 5(a)).

Next, from the near field radiated by the equivalent currents reconstructed on C_0', the equivalent currents on C_1' and C_2' are retrieved. Fields due to these equivalent currents reconstructed are plotted in Fig. 5(c). Once again, fields outside the reconstruction domains C_1' and C_2' match Fig. 5(a) results.

Figures 5(e) and 5(d) represent the fields radiated by the equivalent currents $\vec{J}_{eq}(\vec{\rho}_1')$ and $\vec{M}_{eq}(\vec{\rho}_1')$ reconstructed on C_1' (horn antenna), and $\vec{J}_{eq}(\vec{\rho}_2')$ and $\vec{M}_{eq}(\vec{\rho}_2')$ reconstructed on C_2' (metallic plate), respectively. In the case of Fig. 5(e) results, it can be appreciated that the blockage due to the presence of the metallic plate is almost removed.

In order to provide a quantitative comparison of the results, the radiation pattern of the horn antenna is plotted in Fig. 6 (black dashed line). This pattern is compared with that one distorted due

to the presence of the metallic plate (green line, $\vec{E}_{scatt}$), together with the radiation pattern calculated from $\vec{J}_{eq}(\vec{\rho}_1')$ and $\vec{M}_{eq}(\vec{\rho}_1')$ (blue line, $\vec{E}_{scatt,1}$), and $\vec{J}_{eq}(\vec{\rho}_2')$ and $\vec{M}_{eq}(\vec{\rho}_2')$ (red line, $\vec{E}_{scatt,2}$). It can be appreciated that the radiation pattern corresponding to $\vec{J}_{eq}(\vec{\rho}_1')$ and

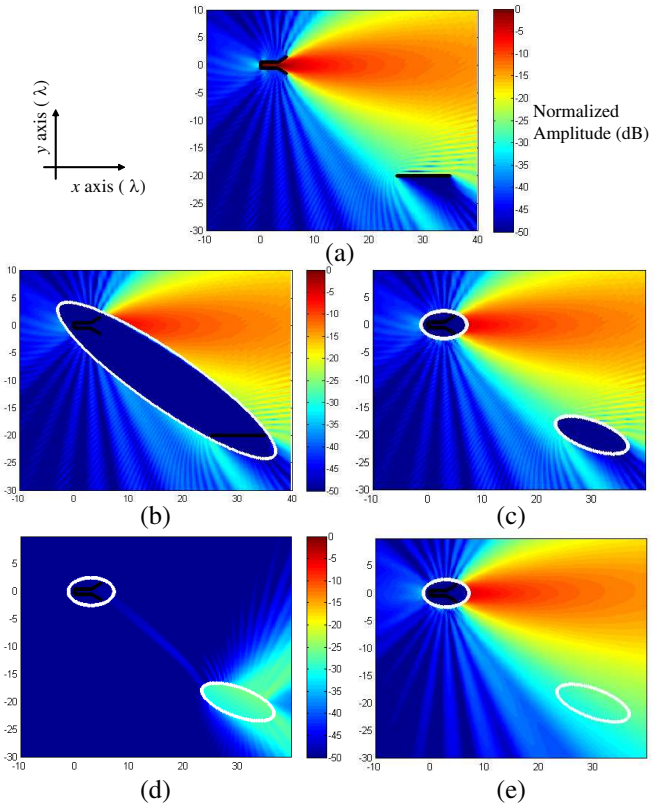

Figure 5. Field distribution (normalized amplitude, in dB). (a) Original problem: AUT and metallic scatterer. (b) Field radiated by the equivalent currents reconstructed on the contour C_0' enclosing all the radiators and scatterers. (c) Field radiated by the equivalent currents reconstructed on the contours enclosing the AUT (C_1') and the metallic plate (C_2'). (d) Field radiated by the equivalent currents reconstructed on the contour enclosing the metallic plate (C_2'). (e) Field radiated by the equivalent currents reconstructed on the contour enclosing the AUT (C_1'). Black line: AUT and metallic plate. White line: reconstruction domains.

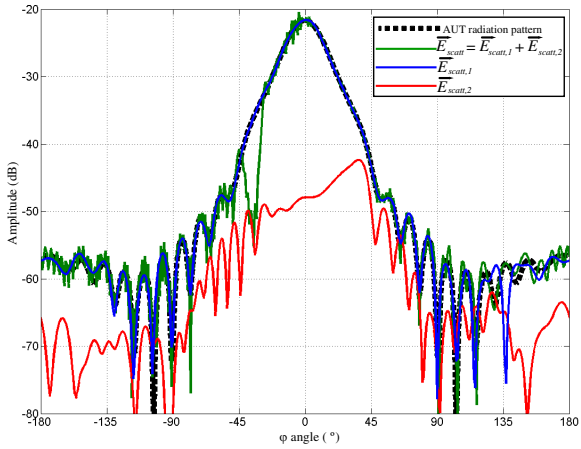

Figure 6. Comparison of the radiation pattern (amplitude, in dB) calculated from the reconstructed equivalent currents with the AUT radiation pattern.

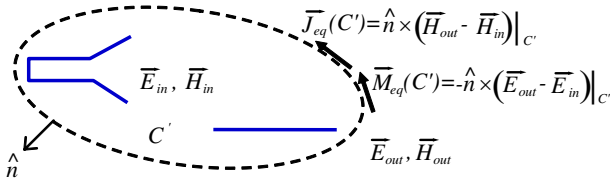

Figure 7. Antenna characterization in terms of equivalent currents.

$\vec{M}_{eq}(\vec{\rho}_1')$ (blue line) almost matches the non-distorted horn radiation pattern (the ripple and the $-40°$ null caused by the multipath interference is removed).

Another interesting comparison is related to the equivalent currents and the tangential field components on the reconstruction domains. According to the Equivalence Principle, the equivalent currents on the reconstruction domain (Fig. 7) satisfy (7):

$$\left.\begin{aligned} \vec{J}_{eq}(C') &= \hat{n} \times \left(\vec{H}_{out} - \vec{H}_{in}\right)\Big|_{C'} \\ \vec{M}_{eq}(C') &= -\hat{n} \times \left(\vec{E}_{out} - \vec{E}_{in}\right)\Big|_{C'} \end{aligned}\right\} \tag{7}$$

When the zero internal field condition ($\vec{E}_{in} = 0$, $\vec{H}_{in} = 0$) is enforced (Love's Equivalence Principle [11, 12]) (8):

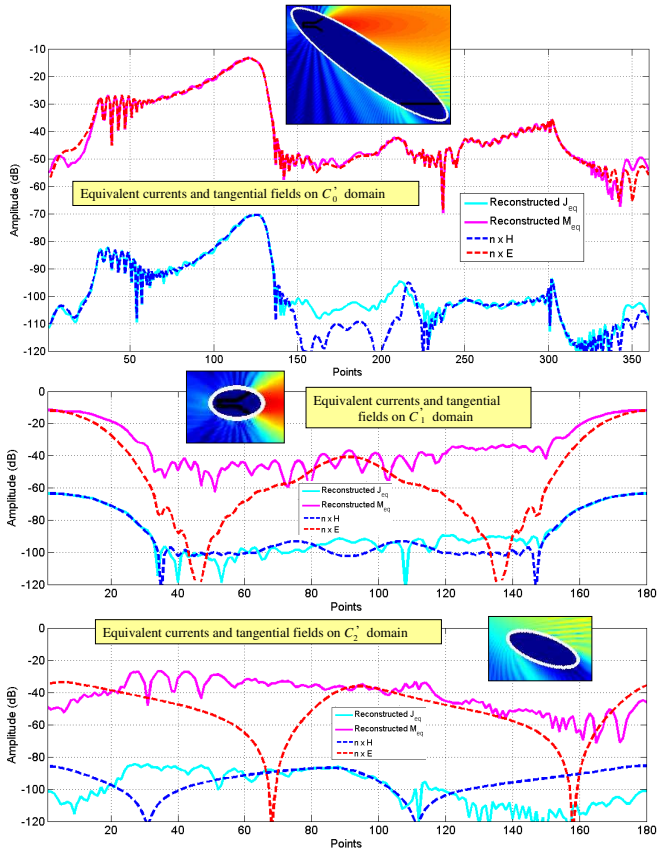

Figure 8. Reconstructed equivalent currents and tangential fields on the reconstruction domains. Top: C_0' domain. Center: C_1' domain. Bottom: C_2' domain.

$$\left.\begin{aligned} \vec{J}_{eq}(C') &= \hat{n} \times \vec{H}_{out}\Big|_{C'} \\ \vec{M}_{eq}(C') &= -\hat{n} \times \vec{E}_{out}\Big|_{C'} \end{aligned}\right\} \tag{8}$$

Using the 2D-MoM analysis, the tangential fields on C_0', C_1' and C_2' domains have been calculated, with the aim of comparing them with the reconstructed equivalent currents on these domains. The comparison is plotted in Fig. 8. It is possible to appreciate a good agreement between the tangential fields and the reconstructed equivalent currents on C_0' domain, while there are some discrepancies in C_1' and C_2', except for the contour corresponding to the horn antenna

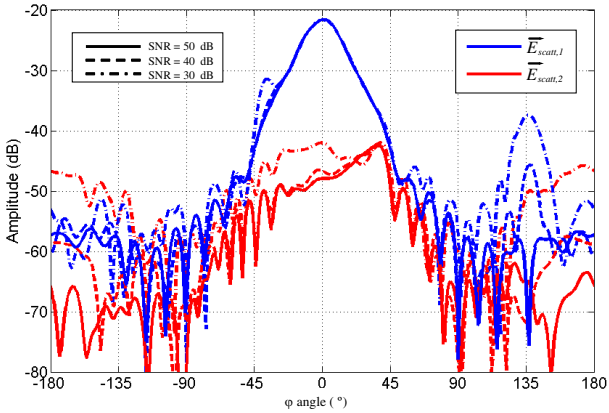

Figure 9. Fields radiated by the reconstructed equivalent currents on C_1' and C_2' when noise is added to the observed field.

main beam (electric and magnetic field levels of -10 and -60 dB respectively).

Method performance in the presence of noise is also analyzed. For this purpose, noise is added to the field acquired in C_{obs} according to different signal-to-noise ratio (SNR). As shown in Fig. 9, the method is able to recover the horn antenna pattern when the SNR is up to 40 dB. When noise is added according to a SNR of 30 dB, it can be noticed that the predicted fields do not match the correct ones. This distortion is also shown in Fig. 10, where the fields calculated from the reconstructed equivalent currents (when SNR is 30 dB) are plotted.

Finally, the influence of the sampling rate on the field observation domain (C_{obs}, a circumference of $R = 50\lambda$) is analyzed. In this case, the minimum radius of the circumference enclosing both the AUT and the metallic plate is $R_0 = 41\lambda$, so according to the field sampling criterion [18] the minimum number of field samples would be Eq. (9):

$$\begin{aligned} N &= \lceil k_0 R_0 + 10 \rceil = 268 \\ \Delta\varphi_{\min} &= 360^\circ/268 \approx 1.35^\circ \end{aligned} \tag{9}$$

Thus, the method is expected to fail if the field sampling rate is larger than $\Delta\varphi_{\min}$. To prove this, the equivalent currents are reconstructed for different sampling rates on the observation domain (C_{obs}). The fields radiated by these equivalent currents are plotted in Fig. 11, showing the method failure when $\Delta\varphi > \Delta\varphi_{\min}$.

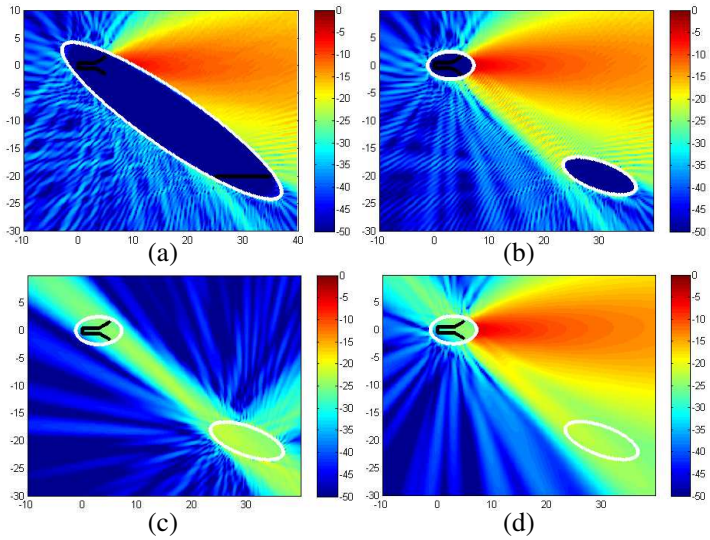

Figure 10. Field distribution (normalized amplitude, in dB) when noise is added to the observed field according to a SNR of 30 dB. (a) Field radiated by the equivalent currents reconstructed on the contour C_0' enclosing all the radiators and scatterers. (b) Field radiated by the equivalent currents reconstructed on the contours enclosing the AUT (C_1') and the metallic plate (C_2'). (c) Field radiated by the equivalent currents reconstructed on the contour enclosing the metallic plate (C_2'). (d) Field radiated by the equivalent currents reconstructed on the contour enclosing the AUT (C_1'). Black line: AUT and metallic plate. White line: reconstruction domains.

3.3. Horn Antenna Mounted onto a Metallic Positioner

The third example presents the method applicability in a real scenario, using a similar setup as the one presented in [5]. A horn antenna is mounted onto an AUT positioner at the spherical range in anechoic chamber of the TSC-UNIOVI research group [19–21]. No absorbents have been placed between the horn antenna and the AUT positioner metallic structure, as depicted in Fig. 12, resulting in a slightly pattern distortion. The horn antenna (AUT) is measured at the working frequency of 17 GHz, and the radiated field is acquired in an observation domain C_{obs} ($R = 5$ m, $\varphi = [-90°, 90°]$ with $\Delta\varphi = 1°$).

First, an equivalent currents distribution is reconstructed on an elliptical domain (C_0') enclosing both the horn antenna aperture and the metallic structure, as shown in Fig. 13(a). It can be appreciated

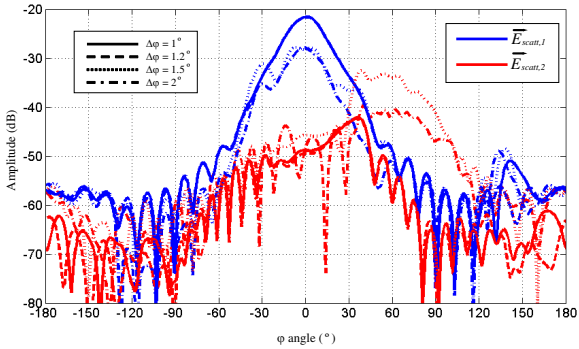

Figure 11. Fields radiated by the reconstructed equivalent currents on C_1' and C_2' for different sampling rates on the observed field.

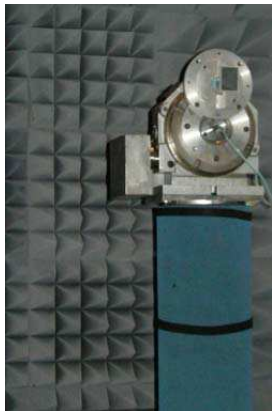

Figure 12. Detail of the horn antenna mounted onto the AUT positioner.

some ripple in the area surrounding the reconstruction domain, due to the interference between the horn antenna and the metallic structure, as well as the fact that the backward radiation is almost zero (80 dB below the maximum) because of the presence of the metallic structure behind the horn antenna.

Once again, the near-field around the reconstruction domain C_0' is calculated, being used to recover the equivalent currents on C_1' and C_2'. C_1' is an elliptical domain enclosing the horn antenna aperture, and C_2' another elliptical domain containing the metallic parts of the AUT positioner.

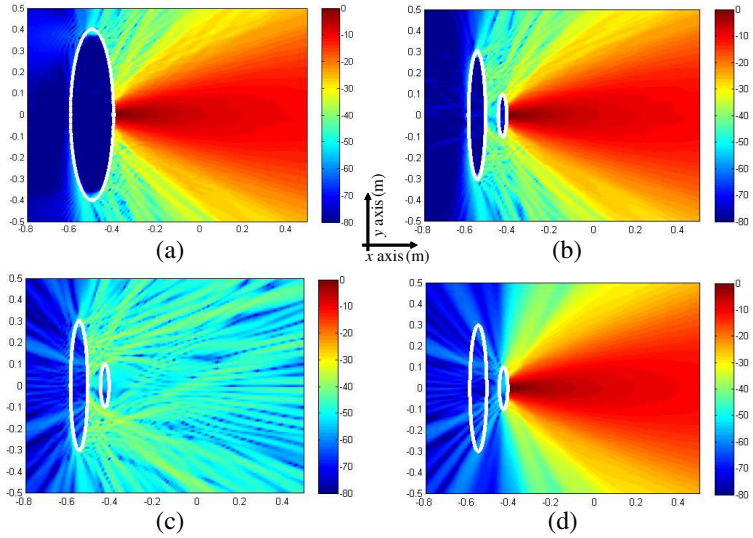

Figure 13. Field distribution (normalized amplitude, in dB). (a) Field radiated by the equivalent currents reconstructed on the contour C_0' enclosing all the radiators and scatterers. (b) Field radiated by the equivalent currents reconstructed on the contours enclosing the AUT (C_1') and the metallic structure (C_2'). (c) Field radiated by the equivalent currents reconstructed on the contour enclosing the metallic structure (C_2'). (d) Field radiated by the equivalent currents reconstructed on the contour enclosing the AUT (C_1'). White line: reconstruction domains.

The fields radiated by equivalent currents reconstructed on C_1' and C_2' are plotted in Fig. 13(b), presenting a good agreement with Fig. 13(a). Fig. 13(c) represents the fields due to reflections on the metallic structures behind the horn antenna, and Fig. 13(d), the contribution from the equivalent currents retrieved on the horn antenna aperture. It can be observed that the ripple due to interaction with the metallic structure is removed.

Pattern comparison is plotted in Fig. 14: first, the measured radiation pattern (dashed black line) is compared with that one calculated from the reconstructed equivalent currents in both domains (green line). Next, the radiated field due to equivalent currents on C_1' and C_2' are calculated separately. It is found that the radiation pattern corresponding to C_1' currents presents a smooth shape, i.e., without the ripple that can be attributable to the reflections on the metallic AUT supporting structure.

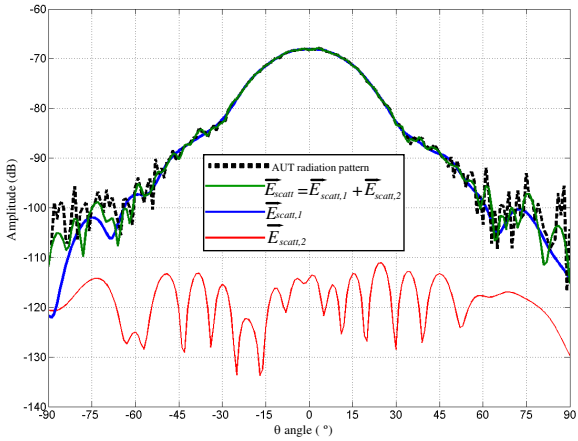

Figure 14. Radiation pattern of the reconstructed equivalent currents, and measured AUT radiation pattern.

4. CONCLUSIONS

From the results presented in the previous section it can be proved the effectiveness of the proposed SRM application for multipath contribution characterization and removal, when working at one single frequency. It has been also studied the method sensitivity to random noise, being able to work with SNR higher than 40 dB. It must be noticed that this SNR value can be only achieved in high-quality measurement facilities, as it requires that all the random and systematic measurement errors must be below this level. Further work will be focused on the method improvement to make it more robust for lower SNR, as well as the benchmarking with UWB-based echo cancellation methods.

ACKNOWLEDGMENT

This work has been supported by the European Union under COST IC0603 ("ASSIST") action; by the "Ministerio de Ciencia e Innovación" of Spain/FEDER under projects TEC2008-01638/TEC (INVEMTA), CONSOLIDER-INGENIO CSD2008-00068 (TERASENSE), and under PhD grant BES-2009-024060; by PCTI Asturias under project PC10-06 (FLEXANT); and by the "Gobierno del Principado de Asturias" under PhD grant BP09139.

REFERENCES

1. Hess, D. W., "Spherical near-field antenna measurements: A review of correction techniques," *2007 Loughborough Antennas and Propagation Conference*, 27–32, 2007.
2. Loredo, S., M. R. Pino, F. Las-Heras Andrés, and T. K. Sarkar, "Echo identification and cancellation techniques for antenna measurement in non-anechoic test sites," *IEEE Antennas and Propagation Magazine*, Vol. 46, No. 1, 100–107, Feb. 2004.
3. Leatherm, P. S. H., J. D. Parsons, J. Romeu, S. Blanch, and A. Aguasca, "Practical validation of antenna pattern measurement interference cancellation using a correlation technique," *2004 IEEE Antennas and Propagation Society International Symposium*, Vol. 1, 735–738, 2004.
4. Moon, J.-I., S.-S. Oh, and Y.-B. Jung, "Echo-cancellation technique with recursive data in nonanechoic test sites," *IEEE Antennas and Wireless Propagation Letters*, Vol. 8, 558–560, 2009.
5. Hess, D. W., "The isofilter^{TM} technique: A method of isolating the pattern of an individual radiator from data measured in a contaminated environment," *IEEE Antennas and Propagation Magazine*, Vol. 52, No. 1, 174–181, Feb. 2010.
6. Marquart, N. P., "Experimental anechoic chamber measurements of a target near an interface," *Progress In Electromagnetics Research*, Vol. 61, 143–158, 2006.
7. Alvarez Lopez, Y., C. Cappellin, F. Las-Heras Andrés, and O. Breinbjerg, "On the comparison of the spherical wave expansion-to-plane wave expansion and the sources reconstruction method for antenna diagnostics," *Progress In Electromagnetics Research*, Vol. 87, 245–262, Nov. 2008.
8. Álvarez, Y., F. Las-Heras Andrés, M. R. Pino, and T. K. Sarkar, "An improved super-resolution sources reconstruction method," *IEEE Trans. on Instrumentation and Measurement*, Vol. 58, No. 11, 3855–3866, Nov. 2009.
9. Álvarez, Y., F. Las-Heras Andrés, B. A. Casas, and C. García, "Antenna diagnostics using arbitrary-geometry field acquisition domains," *IEEE Antennas and Wireless Propagation Letters*, Vol. 8, 375–378, 2009.
10. Persson, K. and M. Gustafson, "Reconstruction of equivalent currents using a near-field data transformation — with radome application," *Progress in Electromagnetics Research*, Vol. 54, 179–198, 2005.
11. Quijano, J. L. A. and G. Vecchi, "Improved-accuracy source

reconstruction on arbitrary 3-D surfaces," *IEEE Antennas and Wireless Propagation Letters*, Vol. 8, 1046–1049, 2009.

12. Quijano, J. L. A. and G. Vecchi, "Field and source equivalence in source reconstruction on 3D surfaces" *Progress In Electromagnetics Research*, Vol. 103, 67–100, 2010.
13. Laviada-Martinez, J., Y. Alvarez Lopez, and F. Las-Heras Andrés, "Efficient determination of the near-field in the vicinity of an antenna for the determination of its safety perimeter," *Progress In Electromagnetics Research*, Vol. 103, 371–391, 2010.
14. Las-Heras Andrés, F., "Using equivalent currents to analyze antennas in complex environments," *Microwave and Optical Technology Letters*, Vol. 31, No. 1, Oct. 2001.
15. Balanis, C. A., *Advanced Engineering Electromagnetics*, John Wiley & Sons, New York, 1989.
16. Roger, A. and F. Chapel, "Iterative methods for inverse problems," *Progress In Electromagnetics Research*, Vol. 5, 423–454, 1991.
17. Carpentieri, B., "Fast iterative solution methods in electromagnetic scattering," *Progress In Electromagnetics Research*, Vol. 79, 151–178, 2008.
18. Hansen, J. E., *Spherical Near-Field Antenna Measurements*, Peter Peregrinus Ltd. London, 1988.
19. De Cos, M. E., Y. Álvarez Lopez, and F. Las-Heras Andrés, "Planar artificial magnetic conductor: Design and characterization setup in the RFID SHF band," *Journal of Electromagnetic Waves and Applications*, Vol. 23, Nos. 11–12, 1467–1478, 2009.
20. De Cos, M. E., Y. Álvarez Lopez, and F. Las-Heras Andrés, "A novel approach for RCS reduction using a combination of artificial magnetic conductors," *Progress In Electromagnetics Research*, Vol. 107, 147–159, 2010.
21. De Cos, M. E., Y. Álvarez Lopez, R. C. Hadarig, and F. Las-Heras Andrés, "Flexible Uniplanar Artificial Magnetic Conductor," *Progress In Electromagnetics Research*, Vol. 106, 349–362, 2010.